

# AGZO: Activation-Guided Zeroth-Order Optimization for LLM Fine-Tuning

Wei Lin<sup>1</sup> Yining Jiang<sup>2</sup> Qingyu Song<sup>2</sup> Qiao Xiang<sup>2</sup> Hong Xu<sup>1</sup>

## Abstract

Zeroth-Order (ZO) optimization has emerged as a promising solution for fine-tuning LLMs under strict memory constraints, as it avoids the prohibitive memory cost of storing activations for backpropagation. However, existing ZO methods typically employ isotropic perturbations, neglecting the rich structural information available during the forward pass. In this paper, we identify a crucial link between gradient formation and activation structure: the gradient of a linear layer is confined to the subspace spanned by its input activations. Leveraging this insight, we propose Activation-Guided Zeroth-Order optimization (AGZO). Unlike prior methods, AGZO extracts a compact, activation-informed subspace on the fly during the forward pass and restricts perturbations to this low-rank subspace. We provide a theoretical framework showing that AGZO optimizes a subspace-smoothed objective and provably yields update directions with higher cosine similarity to the true gradient than isotropic baselines. Empirically, we evaluate AGZO on Qwen3 and Pangu models across various benchmarks. AGZO consistently outperforms state-of-the-art ZO baselines and significantly narrows the performance gap with first-order fine-tuning, while maintaining almost the same peak memory footprint as other ZO methods.

## 1. Introduction

Large language models (LLMs) are increasingly adapted to downstream tasks via fine-tuning, but in many practical settings—especially outside large-scale compute clusters—fine-tuning is primarily constrained by GPU memory (Hu et al., 2022; Ouyang et al., 2022). A key reason is that backpropagation requires storing forward activations (and related intermediate tensors), which can dominate the peak foot-

print at large sequence lengths and batch sizes (Chen et al., 2016; Rajbhandari et al., 2020). Zeroth-order (ZO) optimization provides an appealing alternative in such memory-limited regimes. ZO methods bypass backpropagation by updating parameters using only function evaluations, typically employing randomized finite-difference estimators to approximate the gradient (Nesterov & Spokoiny, 2017; Ghadimi & Lan, 2013; Duchi et al., 2015). Specifically, MeZO adapts two-point randomized finite differences to LLM fine-tuning (Malladi et al., 2023). By employing in-place parameter perturbations and regenerating noise from random seeds, it achieves a peak memory footprint comparable to inference alone. This line of work demonstrates that ZO methods make end-to-end fine-tuning feasible under stricter hardware constraints, substantially reducing training memory while maintaining acceptable performance levels (Sun et al., 2022; Chen et al., 2023; Zhang et al., 2024).

Despite this progress, existing ZO fine-tuning baselines all follow a *black-box perturbation* paradigm: perturbations are sampled from data-independent Gaussian distributions defined solely by parameter dimensions. MeZO uses isotropic full-space perturbations (Malladi et al., 2023), and recent variant LOZO explores low-rank perturbations motivated by spectral properties of gradients (Chen et al., 2025b). Across these approaches, the perturbation distribution is typically independent of the internal representations produced by the current forward pass. This is a missed opportunity, as the forward evaluation exposes structural information that is intrinsically linked to the true gradient direction.

This paper is motivated by a simple observation about backpropagation in linear layers of LLMs: the weight gradient on a mini-batch is completely determined by the upstream signals flowing into the layer and the activations produced in the forward pass. As a consequence, the gradient directions of a linear layer are confined to the subspace spanned by the mini-batch activations, rather than being arbitrary in the full parameter space. In parallel, a growing body of empirical and theoretical work suggests that adaptation during fine-tuning is effectively low-dimensional and often admits low-rank structure, which has been exploited by parameter-efficient and low-rank update methods (Aghajanyan et al., 2021; Li et al., 2018; Hu et al., 2022; Hao et al., 2024). These insights motivate a simple principle for ZO fine-tuning: instead of perturbing weights in unconstrained

<sup>1</sup>Department of Computer Science and Engineering, The Chinese University of Hong Kong, Hong Kong <sup>2</sup>Xiamen University, China. Correspondence to: Hong Xu <hongxu@cuhk.edu.hk>.

random directions, one should concentrate perturbations within an activation-informed low-dimensional subspace revealed by the forward pass.

Guided by this principle, we propose Activation-Guided Zeroth-Order optimization (AGZO). Each iteration of AGZO starts with the standard forward pass, which both evaluates the loss and produces the mini-batch activations. For each linear layer, AGZO then computes a compact set of dominant activation directions using a lightweight power iteration process (Golub & Van Loan, 2013; Miyato et al., 2018). AGZO samples low-rank, activation-guided perturbations constrained to this subspace, and uses them to form the usual forward-only ZO update. For nonlinear trainable layers, AGZO falls back to standard Gaussian perturbations to preserve general applicability across architectures. Crucially, AGZO does not retain activations across iterations: activations are discarded immediately after subspace extraction, and only compact subspace information is kept, thereby maintaining the memory advantages of ZO fine-tuning. Compared with existing perturbation baselines, AGZO exploits per-iteration activation structure to construct more informative perturbations, improving update quality while retaining the same memory efficient character.

We provide a theoretical framework explaining the efficacy of activation guidance. By analyzing the alignment between the estimated and true gradients, we prove that AGZO generates update directions that are provably closer to the true gradient than those produced by random full-space perturbation baselines. We interpret AGZO as optimizing a subspace-smoothed objective and analyze how well its estimator aligns with the true gradient in expectation. Under an activation spectral concentration condition—formalizing that most gradient energy lies in the leading singular directions of the activation matrix (Gur-Ari et al., 2018; Papyan, 2020)—we show that AGZO achieves a larger expected cosine similarity to the true gradient than full-space random perturbation baseline. This result formalizes the intuition that activation-informed subspaces focus the optimization on directions carrying meaningful gradient signals, thereby enhancing the effectiveness of each update step.

We evaluate AGZO on Qwen3 (Yang et al., 2025) and Pangu (Chen et al., 2025a) models under practical GPU memory constraints. AGZO consistently outperforms MeZO and LOZO on various downstream benchmarks, narrowing the gap to first-order fine-tuning. We further support our motivation and theory by directly measuring directional fidelity, where AGZO achieves consistently higher cosine similarity to the true gradients than prior ZO baselines. Finally, we compare peak GPU memory usage by sweeping across sequence lengths and batch sizes, and show that AGZO matches the memory profile of other forward-only ZO baselines while remaining far below first-order training.

The primary contributions of this work are as follows:

- We identify and formalize a fundamental structural link between gradients and activations in linear layers and empirically demonstrate that, during LLM fine-tuning, the gradient signal concentrates in a low-dimensional subspace revealed by the forward-pass activations.
- Building on this insight, we propose AGZO, a zeroth-order fine-tuning method that extracts compact activation subspaces on the fly and uses them to construct low-rank, activation-guided perturbations.
- We develop a principled theoretical framework that explains why activation guidance improves ZO optimization. We show that AGZO can be viewed as optimizing a subspace-smoothed objective, and its update directions are provably more aligned with the true gradient than random perturbation methods under activation spectral concentration.
- We conduct experiments on Qwen3 models that jointly demonstrate (i) improved end-to-end fine-tuning performance over prior ZO baselines, (ii) consistently stronger gradient alignment with the true backpropagation direction, and (iii) a peak GPU memory footprint that remains essentially unchanged relative to standard forward-only ZO methods across varying batch size and sequence length.

## 2. Background: Zeroth-Order Fine-Tuning Baselines

We consider the standard stochastic optimization problem

$$\min_{W \in \mathbb{R}^d} F(W) \triangleq \mathbb{E}_{B \sim \mathcal{D}} [f(W; B)], \quad (1)$$

where  $W$  denotes the parameters of a LLM,  $\mathcal{D}$  is a data distribution over minibatches  $B$ , and  $f(W; B)$  is the empirical loss. First-order methods estimate  $\nabla F(W)$  via backpropagation, which requires storing forward activations and thus dominates the training memory footprint. Zeroth-order methods approximate gradient directions using only function evaluations and avoid backpropagation, making them attractive for memory-limited fine-tuning of large models (Zhang et al., 2024; Malladi et al., 2023). In this section we briefly review two representative ZO baselines for LLM fine-tuning: MeZO and LOZO (Malladi et al., 2023; Chen et al., 2025b).

### 2.1. MeZO: Memory-Efficient Full-Space Perturbations

MeZO adapts classical Gaussian-smoothing ZO estimators to the LLM fine-tuning setting. Let  $u \sim \mathcal{N}(0, I_d)$  be a standard Gaussian perturbation, organized layer-wise as

$u = (U_1, \dots, U_L)$  where each  $U_\ell$  has the same shape as  $W_\ell$ . Given a smoothing parameter  $\mu > 0$  and a minibatch  $B$ , MeZO performs two forward passes to evaluate  $f(W + \mu u; B)$  and  $f(W; B)$  and constructs the finite difference estimator

$$\hat{g}_\mu^{\text{MeZO}}(W; B) = \frac{f(W + \mu u; B) - f(W; B)}{\mu} u. \quad (2)$$

This estimator can be interpreted as the gradient of a Gaussian-smoothed objective  $F_\mu(W) = \mathbb{E}_u[F(W + \mu u)]$  and is used as a surrogate gradient in a standard optimizer.

To remain memory efficient, MeZO never stores the full perturbation tensor  $u$  explicitly: it perturbs parameters in place and records only the random seed needed to regenerate  $u$  when forming Eq (2). This design reduces fine-tuning memory by roughly a factor of four relative to first order methods while maintaining competitive performance on downstream tasks (Zhang et al., 2024; Gautam et al., 2024). However,  $u$  is supported on the entire parameter space, and empirical studies suggest that layer-wise gradients in LLMs are effectively low-rank (Aghajanyan et al., 2021; Li et al., 2018; Chen et al., 2025b). Full-space isotropic perturbations may spend a substantial portion of the query budget exploring directions that carry little gradient energy.

## 2.2. LOZO: Low-Rank Zeroth-Order Estimation

LOZO aims to better match the observed low-rank structure of gradients by introducing a matrix-wise low-rank ZO estimator (Chen et al., 2025b). For each layer  $\ell$ , LOZO samples random Gaussian factors  $U_\ell \in \mathbb{R}^{d_{\text{out}} \times r_\ell}$  and  $V_\ell \in \mathbb{R}^{d_{\text{in}} \times r_\ell}$  with  $r_\ell \ll \min\{d_{\text{out}}, d_{\text{in}}\}$ , and forms the rank- $r_\ell$  perturbation

$$\Delta_\ell = U_\ell V_\ell^\top, \quad (3)$$

so that the full perturbation is  $\Delta = (\Delta_1, \dots, \Delta_L)$ . LOZO defines the low-rank gradient estimator (LGE) as

$$\hat{g}_\mu^{\text{LOZO}}(W; B) = \frac{F(W + \mu \Delta; B) - F(W; B)}{\mu} \frac{\Delta}{r}, \quad (4)$$

where  $r = \{r_\ell\}_{\ell=1}^L$  and the division is understood layer-wise as  $\Delta_\ell/r_\ell$ . For each layer  $\ell$ , the estimate  $\hat{g}_\mu^{\text{LOZO}}(W; B)_\ell$  has rank at most  $r_\ell$ . Compared with MeZO, LOZO enforces a low-rank structure that more closely resembles FO gradients in LLM fine-tuning. At the same time, the additional memory cost is small: only the factors  $U_\ell$  and  $V_\ell$  (or their random seeds) need to be stored to reconstruct  $\Delta_\ell$ . This makes LOZO a natural low-rank ZO baseline for large-scale fine-tuning.

## 2.3. Limitations of Existing ZO Baselines

In both MeZO and LOZO, the perturbation distribution is determined entirely by parameter shapes and random seeds.

The isotropic directions  $u$  in MeZO and the low-rank factors  $U_\ell, V_\ell$  in LOZO are sampled from fixed distributions and remain independent of what happens inside the network during the forward pass.

This raises a natural question: can we leverage the intermediate information produced by the forward pass to construct more informative perturbation directions, and hence better zeroth-order gradient approximations? In the next section we analyze the relationship between gradients and activations in LLMs and use these insights to derive design principles for our activation-guided ZO method.

## 3. Gradient and Activation Structure as Motivation

This section analyzes the structural properties of gradients in linear layers, revealing both determining links to forward activations and inherent low-rank characteristics. We show that (i) gradients of linear layers admit a simple matrix factorization involving the activation matrices, (ii) both gradients and activations exhibit strong low-rank behavior, and (iii) the gradient row-space is almost entirely contained in the activation column space. These observations motivate constructing zeroth-order perturbations inside an *activation-informed* low-rank subspace rather than in the full parameter space.

### 3.1. Notation and Layer-Wise Gradient Forms

We focus on linear layers in LLMs, such as the projection matrices within self-attention mechanisms and fully connected layers in feed-forward networks. These layers dominate the model scale, accounting for most of the trainable parameters in many architectures (Kaplan et al., 2020; Vaswani et al., 2017; Yang et al., 2025). Consider a network with  $L$  layers and linear parameters  $W_1, \dots, W_L$ .

In Transformer-based architectures, the input consists of a minibatch of sequences. Let  $b$  denote the batch size and  $T$  the sequence length. For a linear layer  $\ell$  with weight matrix  $W_\ell \in \mathbb{R}^{d_{\text{out}} \times d_{\text{in}}}$ , the layer operates position-wise on the token representations. Let  $h_{\ell,t}^{(i)} \in \mathbb{R}^{d_{\text{in}}}$  denote the input activation for the  $t$ -th token of the  $i$ -th sequence ( $1 \leq i \leq b, 1 \leq t \leq T$ ). The pre-activation output  $z_{\ell,t}^{(i)}$  is given by:

$$z_{\ell,t}^{(i)} = W_\ell h_{\ell,t}^{(i)}. \quad (5)$$

Let  $q_{\ell,t}^{(i)} = \partial f / \partial z_{\ell,t}^{(i)}$  denote the upstream gradient with respect to the pre-activation for that specific token. By the chain rule, the gradient of the loss with respect to  $W_\ell$  is the sum of contributions from all tokens in the minibatch:

$$\nabla_{W_\ell} f(W; B) = \sum_{i=1}^b \sum_{t=1}^T q_{\ell,t}^{(i)} (h_{\ell,t}^{(i)})^\top. \quad (6)$$

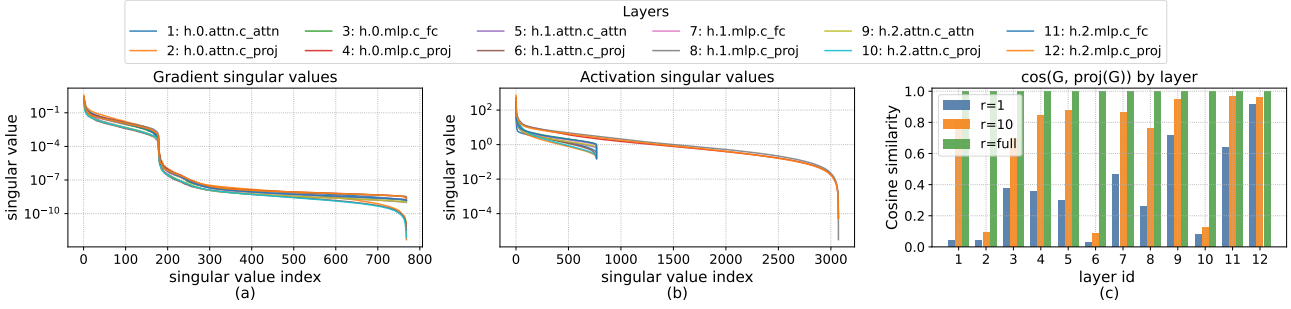


Figure 1. Structural analysis of gradients and activations. (a) & (b) Singular value spectra of gradients and activations. (c) Cosine similarity between the true gradient and its projection onto the activation subspace.

To express this in compact matrix form, we conceptually flatten the batch and sequence dimensions into a single dimension  $m = b \times T$ , representing the total number of tokens in the minibatch. We define the aggregated activation matrix  $H_\ell \in \mathbb{R}^{d_{in} \times m}$  and gradient matrix  $Q_\ell \in \mathbb{R}^{d_{out} \times m}$  by concatenating the column vectors for all tokens:

$$H_\ell = [h_{\ell,1}^{(1)}, \dots, h_{\ell,T}^{(b)}], Q_\ell = [q_{\ell,1}^{(1)}, \dots, q_{\ell,T}^{(b)}], \quad (7)$$

so that the minibatch gradient takes the matrix form

$$\nabla_{W_\ell} f(W; B) = Q_\ell H_\ell^\top, \quad (8)$$

which implies that the row-space of the layer-wise gradient is contained in the column space of the corresponding activation matrix:

$$\text{row}(\nabla_{W_\ell} f(W; B)) \subseteq \text{col}(H_\ell). \quad (9)$$

To quantify how tightly the gradient concentrates in this activation subspace, Fig. 1(c) plots a bar chart of the cosine similarity between the true gradient and its orthogonal projection onto the subspace spanned by the forward activations. Results are obtained when fine-tuning GPT-2 (Radford et al., 2019) on the SST-2 dataset (Wang et al., 2018). Concretely, we perform an SVD of the activation matrix  $H_\ell$  and use the leading  $r$  singular vectors to define a rank- $r$  activation subspace; we then project the gradient onto this subspace and compute the cosine similarity between the original gradient and the projected one. We report results for  $r = 1, 10$  and for the full activation subspace ( $r = 750$ ). Across layers, the cosine similarity is typically close to 1 when  $r \geq 10$ , indicating that almost all gradient energy lies in the subspace spanned by the forward activations.

### 3.2. Low-Rank Structure of Gradients and Activations

The matrix factorization in Eq. (8) reveals the structural dependency of gradients on forward activations. While the weight matrices  $W_\ell$  typically reside in high-dimensional spaces, empirical observations suggest that the actual information content typically concentrates in a much smaller subspace.

To examine this structure more concretely, we compute the singular values of  $\nabla_{W_\ell} f(W; B)$  via SVD and plot them (on a log scale) for a few representative layers and training steps. Figure 1(a) shows that the singular values decay rapidly: the spectrum is far from flat, and a small number of leading singular directions dominate the rest. This supports the view that layer-wise gradients are effectively low-rank.

We observe a similar spectral phenomenon for the forward activation matrices. For each  $H_\ell$ , we compute its singular values and visualize them in Figure 1(b). Again, the singular values exhibit pronounced decay, indicating that the majority of the activation energy is concentrated along a few dominant directions.

Together with the overlap ratios  $\rho_\ell$  in Figure 1(c), these results show that layer-wise gradient information is concentrated in a low-dimensional subspace that is almost entirely determined by the corresponding activation matrix, and that this activation subspace itself has a rapidly decaying spectrum and can be captured by a small number of leading directions. From a zeroth-order perspective, it is therefore natural to restrict perturbations to a low-rank subspace extracted from forward activations, rather than sampling arbitrary directions in the full parameter space. In the next section we instantiate this idea in an activation-guided ZO method that constructs perturbations inside such activation-informed subspaces.

## 4. Activation-Guided Zeroth-Order Optimization

We now introduce Activation-Guided Zeroth-Order optimization (AGZO). For linear layers, AGZO perturbs weights inside an activation-guided low-rank subspace; for non-linear layers, AGZO simply uses full Gaussian perturbations as in MeZO. Each iteration reuses the standard forward pass to both evaluate the loss and extract dominant activation directions, without storing activation matrices across iterations.

**Algorithm 1** SUBSPACEEXTRACT( $H, r, K$ ): activation-informed basis via power iteration

---

```

1: Input: activation matrix  $H \in \mathbb{R}^{d_{\text{in}} \times m}$ , target rank  $r$ , number of power-iteration steps  $K$ 
2: Sample Gaussian test matrix  $\Omega \in \mathbb{R}^{m \times r}$ 
3:  $Y \leftarrow H\Omega$ 
4: for  $k = 1, \dots, K$  do
5:    $[Q, \sim] \leftarrow \text{qr}(Y)$            // orthonormalize columns
6:    $Y \leftarrow H(H^\top Q)$ 
7: end for
8:  $[Q, \sim] \leftarrow \text{qr}(Y)$ 
9: return  $A \leftarrow Q$            //  $A \in \mathbb{R}^{d_{\text{in}} \times r}$ 

```

---

#### 4.1. AGZO Algorithm

Consider a linear layer  $\ell$  with weight matrix  $W_\ell \in \mathbb{R}^{d_{\text{out}} \times d_{\text{in}}}$  and activation matrix  $H_\ell \in \mathbb{R}^{d_{\text{in}} \times m}$  for the current minibatch, as in Section 3.1. AGZO constructs, on the fly, an activation-informed subspace from  $H_\ell$  and samples perturbations inside this subspace.

**Activation-informed subspace.** Given a target rank  $r \ll \min\{d_{\text{out}}, d_{\text{in}}, m\}$ , we approximate the top  $r$  left singular vectors of  $H_\ell$  via a few steps of power iteration on  $H_\ell H_\ell^\top$ , using only matrix–matrix products with  $H_\ell$  and  $H_\ell^\top$ . The routine in Algorithm 1 takes the current activation matrix  $H$  and returns an orthonormal basis  $A \in \mathbb{R}^{d_{\text{in}} \times r}$  whose columns span a rank- $r$  subspace of  $\text{col}(H)$ . Once  $A_\ell$  is computed for the current minibatch,  $H_\ell$  itself is discarded.

**Perturbations and zeroth order estimator.** Given  $A_\ell \in \mathbb{R}^{d_{\text{in}} \times r_\ell}$ , AGZO samples a low-rank perturbation for each linear layer by drawing a left factor  $R_\ell \in \mathbb{R}^{d_{\text{out}} \times r_\ell}$  with i.i.d. standard normal entries and setting

$$\Delta_\ell = \begin{cases} R_\ell A_\ell^\top, & \text{if layer } \ell \text{ is linear,} \\ u_\ell, & \text{if layer } \ell \text{ is nonlinear,} \end{cases} \quad (10)$$

where  $u_\ell$  is a Gaussian perturbation with the same shape as  $W_\ell$ . The full perturbation is then  $\Delta = (\Delta_1, \dots, \Delta_L)$ . For linear layers, each  $\Delta_\ell$  has rank at most  $r$ , and its row space is contained in the activation-informed subspace spanned by  $A_\ell$ .

Given a smoothing parameter  $\mu > 0$  and minibatch  $B$ , we first evaluate

$$f_0 = f(W; B), \quad (11)$$

and, during this forward pass, compute  $\{A_\ell\}$  for all linear layers using Algorithm 1. We then form  $\Delta$  via (10), evaluate the perturbed loss

$$f_+ = f(W + \mu\Delta; B), \quad (12)$$

**Algorithm 2** AGZO Iteration

---

```

1: Input: Weights  $W$ , ranks  $\{r_\ell\}$ , scalars  $\mu, \eta, K$ .
2: 1. Forward & Subspace Extraction (via Hooks):
3: Run forward pass on batch  $B$  to compute  $f_0$ .
4: During computation at each linear layer  $\ell$ : Extract  $A_\ell \leftarrow \text{SUBSPACEEXTRACT}(H_\ell, r_\ell, K)$ .
5: 2. In-Place Perturbation:
6: for layer  $\ell = 1 \dots L$  do
7:   Sample random seed  $s_\ell$ .
8:   if layer  $\ell$  is linear then
9:     Generate  $R_\ell \sim \mathcal{N}(0, I)$  from  $s_\ell$ ; Set update matrix  $\Delta_\ell = R_\ell A_\ell^\top$ .
10:  else
11:    Generate  $\Delta_\ell \sim \mathcal{N}(0, I)$  from  $s_\ell$ .
12:  end if
13:   $W_\ell \leftarrow W_\ell + \mu\Delta_\ell$  {Apply perturbation in-place}
14: end for
15: 3. Gradient Estimate & Update:
16: Compute  $f_+ = f(W; B)$  with perturbed weights.
17: Set projected gradient scaler  $g \leftarrow (f_+ - f_0)/\mu$ .
18: for layer  $\ell = 1 \dots L$  do
19:   Regenerate  $\Delta_\ell$  using stored seed  $s_\ell$  (and  $A_\ell$  if linear).
20:    $W_\ell \leftarrow W_\ell - \mu\Delta_\ell - \eta \cdot g \cdot \Delta_\ell$  {Restore & Update}
21: end for

```

---

and define the layer-wise estimator

$$\widehat{\nabla}_{W_\ell} f^{\text{AGZO}}(W; B) = \frac{f_+ - f_0}{\mu} \Delta_\ell, \quad \ell = 1, \dots, L. \quad (13)$$

Stacking these matrices across layers yields  $\widehat{g}_\mu^{\text{AGZO}}(W; B)$ , which is used in a ZO gradient descent update.

Algorithm 2 summarizes one AGZO iteration. Subspace extraction for each layer is done immediately when its activation matrix becomes available in the forward pass, so full activations are never stored beyond this step.

In practice we use a very small number of power-iteration steps per layer ( $K = 3$ ), which adds only a few matrix multiplications on top of the forward pass. The dominant cost per iteration is thus forward evaluations, as in MeZO and LOZO.

#### 4.2. Memory Usage

We briefly compare the ZO-specific memory overhead of MeZO, LOZO, and AGZO, ignoring the baseline cost of storing model parameters.

MeZO does not store perturbations and regenerates them from random seeds, incurring essentially no ZO-specific memory overhead. LOZO maintains both  $U_\ell$  and  $V_\ell$ , with memory  $\mathcal{O}((d_{\text{out}} + d_{\text{in}})r_\ell)$  per layer. AGZO only stores the activation-informed bases  $A_\ell$ , with ZO-specific memory

$\mathcal{O}(d_{\text{in}}r)$  per layer; activation matrices are discarded immediately after subspace extraction, and the left factors  $R_\ell$  and perturbations  $\Delta_\ell$  are used only within a single iteration.

In our experiments, we choose  $r_\ell = 1$ , so the number of additional parameters in  $A_\ell$  is negligible compared with the size of the full weight matrix  $W_\ell$  (which has  $d_{\text{out}}d_{\text{in}}$  parameters). Consequently, the extra memory required by AGZO is far smaller than the model memory itself.

## 5. Theoretical analysis of AGZO

We now analyze the AGZO estimator introduced in section 4. The goal is to understand (i) its mathematical essence and how far it is from the true gradient, and (ii) how its directional quality compares to MeZO. We focus on linear layers where AGZO uses low-rank perturbations as in (10) and the zeroth order estimator in (16); layers perturbed with dense Gaussian noise behave as in standard two-point ZO and are omitted from the analysis.

### 5.1. Subspace-smoothing view of AGZO

We first show that AGZO can be interpreted as estimating a projected gradient of a subspace-smoothed objective.

Condition on the subspace bases  $A := \{A_\ell\}$  computed at the current iterate  $W$ . Let  $\Delta(W, R)$  be the random perturbation with layerwise blocks

$$\Delta_\ell(W, R) = R_\ell A_\ell^\top, \quad R_\ell \sim \mathcal{N}(0, I_{m_\ell \times r_\ell}) \text{ i.i.d. across } \ell,$$

and define the subspace-smoothed objective

$$F_{\mu, A}(W) := \mathbb{E}_R [F(W + \mu \Delta(W, R))]. \quad (14)$$

The AGZO estimator for layer  $\ell$  can be written as

$$\widehat{\nabla}_{W_\ell}^{\text{AGZO}}(W; B) = \phi(W, \Delta(W, R); B) R_\ell A_\ell^\top, \quad (15)$$

where

$$\phi(W, \Delta; B) = \frac{f(W + \mu \Delta, B) - f(W, B)}{\mu}. \quad (16)$$

The next proposition shows that, up to smoothing, AGZO is an exact gradient estimator projected onto the activation-informed subspace.

**Proposition 5.1.** *Assume  $F$  is differentiable and the usual interchange of gradient and expectation is valid. Conditioned on  $A$ , the AGZO estimator satisfies, for each linear layer  $\ell$ ,*

$$\mathbb{E}_{R, B} [\widehat{\nabla}_{W_\ell}^{\text{AGZO}}(W; B) \mid A] = \nabla_{W_\ell} F_{\mu, A}(W) A_\ell A_\ell^\top. \quad (17)$$

In particular, AGZO estimates the gradient of the subspace-smoothed objective (14), projected onto  $\text{span}(A_\ell)$ .

*Proof.* See Theorem A.3(b) in Appendix.  $\square$

Under standard smoothness assumptions, the difference between  $\nabla F_{\mu, A}$  and  $\nabla F$  after projection is small.

**Proposition 5.2.** *Suppose  $F$  has  $L$ -Lipschitz gradient. Then for each layer  $\ell$  there exists a constant  $C_\ell > 0$ , depending only on  $L$  and the layer dimensions, such that*

$$\|\nabla_{W_\ell} F_{\mu, A}(W) A_\ell A_\ell^\top - \nabla_{W_\ell} F(W) A_\ell A_\ell^\top\|_F \leq C_\ell \mu. \quad (18)$$

*In particular, the bias from smoothing vanishes linearly as  $\mu \rightarrow 0$  once projected onto  $\text{span}(A_\ell)$ .*

*Proof.* See Theorem A.3(c) in Appendix.  $\square$

The remaining component of the bias comes from projecting  $\nabla_{W_\ell} F(W)$  onto  $\text{span}(A_\ell)$ . Recall the gradient factorization (8) and the subspace analysis (9). In AGZO,  $A_\ell$  is constructed to approximate a low-rank activation subspace for  $\text{col}(H_\ell)$ . For exposition, consider the idealized case where this subspace exactly supports the gradient.

**Corollary 5.3.** *Suppose for a given layer  $\ell$  and all mini-batches  $B$ ,*

$$\text{row}(\nabla_{W_\ell} f(W, B)) \subseteq \text{span}(A_\ell), \quad (19)$$

*so that  $\nabla_{W_\ell} F(W) = \nabla_{W_\ell} F(W) A_\ell A_\ell^\top$ . Then combining (17) and (18) yields*

$$\left\| \mathbb{E}_{R, B} [\widehat{\nabla}_{W_\ell}^{\text{AGZO}}(W; B) \mid A] - \nabla_{W_\ell} F(W) \right\|_F \leq C_\ell \mu. \quad (20)$$

*Thus, in this regime AGZO is an asymptotically unbiased estimator of the true layer gradient as  $\mu \rightarrow 0$ .*

In practice, the activation-guided subspace only approximates the row space. Section 3 shows that the overlap between  $\nabla_{W_\ell} F(W)$  and  $\nabla_{W_\ell} F(W) A_\ell A_\ell^\top$  is nevertheless very close to one if the approximation rank is high enough.

### 5.2. Directional quality and comparison with MEZO

Since the update length can be tuned by step size, the effectiveness of a gradient estimator mainly depends on its directional quality: how well its direction aligns with the true gradient. This subsection analyzes the expected cosine similarity between the estimator and the true gradient, and compares AGZO with MeZO in an idealized noiseless setting.

Let  $G \in \mathbb{R}^{m \times n}$  denote the true gradient  $\nabla_{W_\ell} F(W)$ , and let  $\widehat{G}$  be the approximated gradient. Define the cosine similarity

$$\cos(\widehat{G}, G) := \frac{\langle \widehat{G}, G \rangle_F}{\|\widehat{G}\|_F \|G\|_F}, \quad \langle A, B \rangle_F := \text{tr}(A^\top B). \quad (21)$$

We analyze the expected cosine similarity in a noiseless setting ( $\mu \rightarrow 0$ ) where the finite difference oracle returns exact directional derivatives and stochastic minibatch noise is ignored. In this regime  $\widehat{G}$  becomes a linear function of the Gaussian direction, which allows a closed-form computation.

**AGZO.** For AGZO, focus on a single layer and write  $G \in \mathbb{R}^{m \times n}$  and  $A \in \mathbb{R}^{n \times r}$  (with orthonormal columns) for simplicity. The low-rank perturbation is  $\Delta = RA^\top$  with  $R \sim \mathcal{N}(0, I_{m \times r})$ , and the corresponding estimator in the limit  $\mu \rightarrow 0$  has the form

$$\widehat{G}_0^{\text{AGZO}} = \langle G, \Delta \rangle_F \Delta = \langle G, RA^\top \rangle_F RA^\top. \quad (22)$$

**Theorem 5.4.** Let  $G \in \mathbb{R}^{m \times n}$  be fixed and  $A \in \mathbb{R}^{n \times r}$  have orthonormal columns. Let  $\widehat{G}_0^{\text{AGZO}}$  be the noiseless AGZO estimator constructed from  $\Delta = RA^\top$  with  $R \sim \mathcal{N}(0, I_{m \times r})$ . Then

$$\mathbb{E}_R [\cos(\widehat{G}_0^{\text{AGZO}}, G)] = \beta_{mr} \frac{\|GA\|_F}{\|G\|_F}, \quad (23)$$

where

$$\beta_D := \mathbb{E}[|U_1|], \quad U = (U_1, \dots, U_D) \sim \text{Unif}(\mathbb{S}^{D-1}), \quad (24)$$

depends only on the product dimension  $mr$ . Equivalently,

$$\beta_D = \frac{\Gamma(\frac{D}{2})}{\sqrt{\pi} \Gamma(\frac{D+1}{2})}, \quad (25)$$

and  $\beta_D$  decays on the order of  $1/\sqrt{D}$  as  $D$  increases.

*Proof.* See Appendix A.2.1.  $\square$

The factor  $\|GA\|_F/\|G\|_F$  has a natural geometric interpretation: it is precisely the fraction of gradient Frobenius energy captured by the AGZO subspace, since  $\|GA\|_F = \|GAA^\top\|_F$  (See remark in Appendix). Thus AGZO benefits both from working in a lower effective dimension  $mr$  (through  $\beta_{mr}$ ) and from aligning its perturbation subspace with directions where  $G$  has large energy.

**MEZO.** For the MeZO baseline with full Gaussian directions, the estimator has the same form but with  $A = I_n$  and  $\Delta = R \in \mathbb{R}^{m \times n}$  dense. Theorem 5.4 then yields the following corollary.

**Corollary 5.5.** In the same setting as above, consider the noiseless MeZO estimator  $\widehat{G}_0^{\text{MEZO}}$  constructed from dense Gaussian directions  $\Delta = R$  with  $R \sim \mathcal{N}(0, I_{m \times n})$ . Then

$$\mathbb{E}_R [\cos(\widehat{G}_0^{\text{MEZO}}, G)] = \beta_{mn}, \quad (26)$$

where  $\beta_D$  is as in (24). This corresponds to the special case of Proposition 5.4 with  $A = I_n$  and  $\|GA\|_F/\|G\|_F = 1$ .

**Comparison under activation spectral concentration.** To compare AGZO and MeZO more explicitly, we recall facts about  $\beta_D$  (proved in the appendix).

**Lemma 5.6.** For every integer  $D \geq 2$ , the sequence  $\{\beta_D\}$  is strictly decreasing in  $D$  and satisfies

$$\sqrt{\frac{2}{\pi D}} \leq \beta_D \leq \sqrt{\frac{2}{\pi(D-1)}}. \quad (27)$$

In particular,  $\beta_{mr} \approx c/\sqrt{mr}$  and  $\beta_{mn} \approx c/\sqrt{mn}$  for a constant  $c \approx \sqrt{2/\pi}$ , so working in a much smaller subspace (with  $r \ll n$ ) already improves the expected cosine similarity by a factor around  $\sqrt{n/r}$ .

*Proof.* See Appendix A.2.1.  $\square$

The second ingredient is the energy ratio  $\|GA\|_F/\|G\|_F$ . In the noiseless case, Theorem 5.4 and Corollary 5.5 give that AGZO has larger expected cosine similarity than MeZO if and only if

$$\frac{\|GA\|_F}{\|G\|_F} > \frac{\beta_{mn}}{\beta_{mr}}. \quad (28)$$

By Lemma 5.6, the right-hand side admits the bound

$$\frac{\beta_{mn}}{\beta_{mr}} < \frac{\sqrt{mr}}{\sqrt{mn-1}}, \quad (29)$$

so a sufficient condition for AGZO to outperform MeZO is

$$\left( \frac{\|GA\|_F}{\|G\|_F} \right)^2 > \frac{r}{n-1/m}. \quad (30)$$

For a given layer, let  $H_\ell \in \mathbb{R}^{n_\ell \times b}$  be the activation matrix and

$$H_\ell = U_\ell \Sigma_\ell V_\ell^\top, \quad \Sigma_\ell = \text{diag}(\sigma_{\ell,1}, \dots, \sigma_{\ell,s_\ell}),$$

its compact SVD with rank  $s_\ell$  and singular values  $\sigma_{\ell,1} \geq \dots \geq \sigma_{\ell,s_\ell} > 0$ . The layer gradient admits the factorization  $\nabla_{W_\ell} F(W) = Q_\ell H_\ell^\top$ , and we set

$$B_\ell := V_\ell^\top Q_\ell^\top Q_\ell V_\ell \succeq 0.$$

AGZO chooses  $A_\ell$  as the leading  $r_\ell$  left singular vectors,  $A_\ell = U_\ell^{(r_\ell)}$ . A direct calculation then yields

$$\frac{\|G_\ell A_\ell\|_F^2}{\|G_\ell\|_F^2} = \frac{\sum_{i=1}^{r_\ell} B_{\ell,ii} \sigma_{\ell,i}^2}{\sum_{i=1}^{s_\ell} B_{\ell,ii} \sigma_{\ell,i}^2}, \quad (31)$$

so (30) is equivalent to

$$\frac{\sum_{i=1}^{r_\ell} B_{\ell,ii} \sigma_{\ell,i}^2}{\sum_{i=1}^{s_\ell} B_{\ell,ii} \sigma_{\ell,i}^2} > \frac{r_\ell}{n_\ell - 1/m_\ell}. \quad (32)$$

Table 1. Experiments on Qwen3-0.6b. The best results are shown in bold except for FO.

Task	FO	AGZO	MEZO	LOZO	Zero	ICL
SST2	0.904	<b>0.877</b>	0.858	0.870	0.540	0.510
COPA	0.730	<b>0.740</b>	0.680	0.690	0.570	0.620
CB	0.946	<b>0.892</b>	0.803	0.760	0.410	0.570
BoolQ	0.768	0.724	<b>0.730</b>	0.724	0.646	0.700
MultiRC	0.826	<b>0.756</b>	0.734	0.737	0.518	0.673
RTE	0.808	<b>0.772</b>	0.732	0.743	0.599	0.722
WiC	0.675	<b>0.595</b>	0.573	0.575	0.498	0.523
SQuAD	0.871	<b>0.790</b>	0.779	0.785	0.416	0.414

This expression makes precise the intuition that AGZO benefits when the gradient energy is concentrated in the leading singular directions of the activation matrix.

The following theorem summarizes the consequence of the spectral assumptions we use in the analysis.

**Theorem 5.7.** *Consider a layer with gradient factorization  $\nabla_{W_\ell} F(W) = Q_\ell H_\ell^\top$  and compact SVD  $H_\ell = U_\ell \Sigma_\ell V_\ell^\top$  of rank  $s_\ell < n_\ell$  with singular values  $\{\sigma_{\ell,i}\}_{i=1}^{s_\ell}$ . Let  $A_\ell = U_\ell^{(r_\ell)}$  be the AGZO subspace and  $B_\ell = V_\ell^\top Q_\ell^\top Q_\ell V_\ell$ . If the average of its first  $r$  diagonal entries is not less than the average of all diagonal entries, i.e.,*

$$\frac{1}{r_\ell} \sum_{i=1}^{r_\ell} B_{\ell,ii} \geq \frac{1}{s_\ell} \sum_{i=1}^{s_\ell} B_{\ell,ii}, \quad (33)$$

and that  $H_\ell$  is low-rank, i.e.,  $s_\ell < n_\ell$ . Then

$$\frac{\sum_{i=1}^{r_\ell} B_{\ell,ii} \sigma_{\ell,i}^2}{\sum_{i=1}^{s_\ell} B_{\ell,ii} \sigma_{\ell,i}^2} > \frac{r_\ell}{s_\ell} \geq \frac{r_\ell}{n_\ell - 1/m_\ell}, \quad (34)$$

and hence, in the noiseless single-query setting,

$$\mathbb{E}_R [\cos(\hat{G}_0^{\text{AGZO}}, G_\ell)] > \mathbb{E}_R [\cos(\hat{G}_0^{\text{MEZO}}, G_\ell)]. \quad (35)$$

Moreover, when the singular values  $\{\sigma_{\ell,i}\}$  are more heterogeneous (so that the leading directions carry more weighted energy), the gap in expected cosine similarity becomes larger.

*Proof.* See Appendix A.3.  $\square$

Theorem 5.7 formalize the intuition behind AGZO: for layers whose gradients concentrate in low-rank activation subspaces, AGZO produces gradient estimates that are better aligned in direction than those of a dense Gaussian ZO method such as MeZO, while requiring only low-rank perturbations.

## 6. Experiments

Table 2. Experiments on Pangu-1B. The best results are shown in bold except for FO.

Task	FO	AGZO	MEZO	LOZO	Zero	ICL
SST2	0.822	<b>0.778</b>	0.764	0.720	0.568	0.717
COPA	0.800	<b>0.770</b>	0.750	<b>0.770</b>	0.760	0.750
CB	0.696	<b>0.732</b>	<b>0.732</b>	0.679	0.500	0.446
BoolQ	0.751	<b>0.730</b>	0.699	0.696	0.695	0.735
RTE	0.780	<b>0.736</b>	0.729	0.697	0.581	0.682
WiC	0.657	<b>0.575</b>	0.567	0.563	0.466	0.511
Avg.	0.751	<b>0.720</b>	0.706	0.687	0.595	0.640

This section evaluates AGZO on instruction-tuned language models under memory constraints. The experiments cover multiple tasks, including the SuperGLUE benchmark (Wang et al., 2019) and other datasets. We consider two model scales, Qwen3-0.6B and Pangu-1B, and compare against established zeroth-order baselines (MeZO, LoZO), as well as non-training baselines (zero-shot prompting and in-context learning, denoted as ICL). When feasible, we also include a first-order fine-tuning baseline (FO) using standard backpropagation. For ZO optimizer, we finetune the LLM for 20000 steps, and for FO optimizer, we use 1000 steps.

All experiments are run on an Ubuntu machine equipped with two NVIDIA RTX 3090 GPUs. All ZO methods update the full set of trainable parameters and use the same data preprocessing and evaluation pipeline. For fair comparison, each method is tuned via grid search over its key hyperparameters, and we report the best configuration selected on the validation set.

### 6.1. Alignment to the true gradient

This diagnostic experiment is designed to validate the directional-quality analysis in Section 5. In particular, Section 5 derives a closed-form expression for the expected cosine similarity of AGZO in the noiseless regime (Theorem 5.4) and shows that, under activation spectral concentration, AGZO achieves a strictly larger expected cosine similarity than MeZO (Theorem 5.7).

To empirically test this prediction in a realistic fine-tuning setting, we fine-tune QWEN3-0.6B on SST-2 and track, at training step  $t$ , the cosine similarity between the ZO estimated gradient and the exact backpropagation gradient computed on the same mini-batch. As shown in Figure 2, AGZO consistently yields higher cosine similarity than MEZO throughout training. This observation directly supports the theoretical conclusion that activation-guided low-rank perturbations improve directional alignment relative to dense Gaussian ZO perturbations.

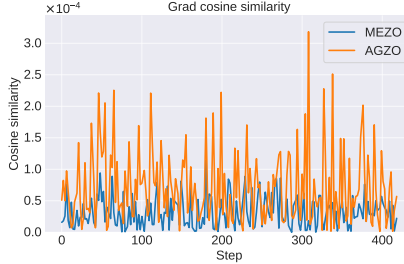
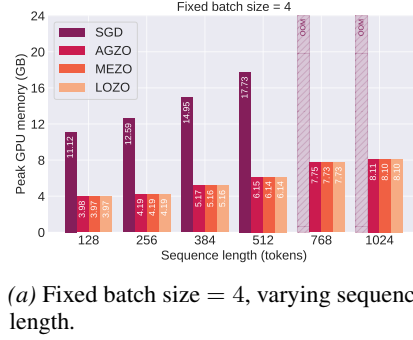
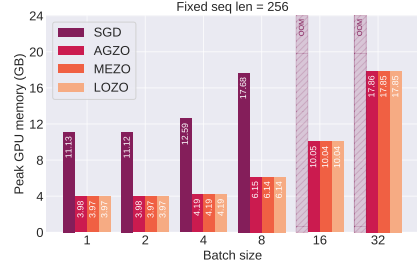


Figure 2. Gradient alignment during fine-tuning.



(a) Fixed batch size = 4, varying sequence length.



(b) Fixed sequence length = 256, varying batch size.

Figure 3. Peak GPU memory usage when fine-tuning Qwen3-0.6B on DROP.

## 6.2. End-to-end fine-tuning performance

**QWEN3-0.6B.** Table 1 shows that AGZO achieves consistently stronger downstream performance than existing ZO baselines across a broad set of benchmarks. This improvement is aligned with the mechanism validated in Section 6.1: by producing update directions that are better aligned with the true gradient, AGZO enables more effective optimization under the same query budget. As a result, AGZO converges to better solutions and noticeably narrows the performance gap between zeroth-order fine-tuning and first-order training.

**PANGU-1B.** Table 2 summarizes the performance of AGZO and various baselines on the OPENPANGU-EMBEDDED-1B model across multiple downstream tasks. Overall, AGZO consistently outperforms existing zeroth-order baselines (MEZO and LOZO) and non-training baselines (zero-shot prompting and in-context learning) on most tasks, demonstrating the effectiveness of our approach in adapting large models with limited gradient information. The average performance shows that AGZO achieves 0.720, surpassing the best ZO baseline (MEZO) by 1.4%.

## 6.3. Peak GPU memory footprint

As discussed in Section 4.2, AGZO only stores the activation-informed basis for each linear layer, without maintaining additional activation state beyond standard ZO state. Since this basis is tiny compared to the weight matrix, AGZO incurs nearly the same peak GPU memory as MEZO.

We empirically validate this memory analysis by measuring the *peak* GPU memory footprint when fine-tuning Qwen3-0.6B and PANGU-1B DROP task. We sweep the two primary drivers of training-time memory: sequence length and batch size. Figure 3 reports two representative slices. In Figures 3(a) and 4a, we fix the batch size to 4 and increase the sequence length. FO (backpropagation) exhibits rapidly growing memory usage and becomes out-of-memory (OOM) at long contexts, whereas AGZO/MEZO/LOZO re-

main substantially lower and continue to run. In Figures 3(b) and 4b, we fix the sequence length to 256 and increase the batch size. FO again hits OOM at moderate batch sizes, while ZO methods remain feasible for significantly larger batches.

Importantly, AGZO matches the memory profile of other forward-only ZO baselines, indicating that the activation-guided subspace construction introduces negligible additional memory overhead.

## 7. Conclusions

We introduced AGZO, a zeroth-order fine-tuning method that leverages per-iteration activation structure to construct low-rank, activation-guided perturbations for linear layers. By extracting compact activation subspaces on the fly via lightweight power iteration, AGZO concentrates ZO updates on directions that are more tightly coupled to backpropagation signals without storing activations across iterations. We provided a principled explanation by interpreting AGZO as optimizing a subspace-smoothed objective and showing that, under activation spectral concentration, its update direction achieves a strictly larger expected cosine similarity to the true gradient than prior ZO baselines. Experiments on Qwen3 models under practical GPU memory constraints corroborate the analysis, demonstrating improved downstream performance and directional fidelity over existing zeroth-order methods while preserving the favorable memory profile of ZO fine-tuning.

## Impact Statement

This paper presents work whose goal is to advance the field of Machine Learning. There are many potential societal consequences of our work, none which we feel must be specifically highlighted here.

## Acknowledgements

This work is supported in part by funding from Huawei (TC20250928057) and CUHK (4937007, 4937008, 5501329, 5501517).

## References

Aghajanyan, A., Gupta, S., and Zettlemoyer, L. Intrinsic dimensionality explains the effectiveness of language model fine-tuning. In *Proceedings of the 59th annual meeting of the association for computational linguistics and the 11th international joint conference on natural language processing (volume 1: long papers)*, pp. 7319–7328, 2021.

Chen, A., Zhang, Y., Jia, J., Diffenderfer, J., Liu, J., Parasyris, K., Zhang, Y., Zhang, Z., Kailkhura, B., and Liu, S. Deepzero: Scaling up zeroth-order optimization for deep model training. *arXiv preprint arXiv:2310.02025*, 2023.

Chen, H., Wang, Y., Han, K., Li, D., Li, L., Bi, Z., Li, J., Wang, H., Mi, F., Zhu, M., et al. Pangu embedded: An efficient dual-system llm reasoner with metacognition. *arXiv preprint arXiv:2505.22375*, 2025a.

Chen, T., Xu, B., Zhang, C., and Guestrin, C. Training deep nets with sublinear memory cost. *arXiv preprint arXiv:1604.06174*, 2016.

Chen, Y., Zhang, Y., Cao, L., Yuan, K., and Wen, Z. Enhancing zeroth-order fine-tuning for language models with low-rank structures. In *The Thirteenth International Conference on Learning Representations*, 2025b. URL <https://openreview.net/forum?id=9BiVepgmWW>.

Duchi, J. C., Jordan, M. I., Wainwright, M. J., and Wibisono, A. Optimal rates for zero-order convex optimization: The power of two function evaluations. *IEEE Transactions on Information Theory*, 61(5):2788–2806, 2015.

Gautam, T., Park, Y., Zhou, H., Raman, P., and Ha, W. Variance-reduced zeroth-order methods for fine-tuning language models. In *Proceedings of the 41st International Conference on Machine Learning*, pp. 15180–15208, 2024.

Ghadimi, S. and Lan, G. Stochastic first-and zeroth-order methods for nonconvex stochastic programming. *SIAM journal on optimization*, 23(4):2341–2368, 2013.

Golub, G. H. and Van Loan, C. F. *Matrix computations*. JHU press, 2013.

Gur-Ari, G., Roberts, D. A., and Dyer, E. Gradient descent happens in a tiny subspace. *arXiv preprint arXiv:1812.04754*, 2018.

Hao, Y., Cao, Y., and Mou, L. Flora: Low-rank adapters are secretly gradient compressors. In *International Conference on Machine Learning*, pp. 17554–17571. PMLR, 2024.

Hu, E. J., Shen, Y., Wallis, P., Allen-Zhu, Z., Li, Y., Wang, S., Wang, L., Chen, W., et al. Lora: Low-rank adaptation of large language models. *ICLR*, 1(2):3, 2022.

Kaplan, J., McCandlish, S., Henighan, T., Brown, T. B., Chess, B., Child, R., Gray, S., Radford, A., Wu, J., and Amodei, D. Scaling laws for neural language models. *arXiv preprint arXiv:2001.08361*, 2020.

Li, C., Farkhoor, H., Liu, R., and Yosinski, J. Measuring the intrinsic dimension of objective landscapes. In *International Conference on Learning Representations*, 2018.

Malladi, S., Gao, T., Nichani, E., Damian, A., Lee, J. D., Chen, D., and Arora, S. Fine-tuning language models with just forward passes. *Advances in Neural Information Processing Systems*, 36:53038–53075, 2023.

Miyato, T., Kataoka, T., Koyama, M., and Yoshida, Y. Spectral normalization for generative adversarial networks. In *International Conference on Learning Representations*, 2018.

Nesterov, Y. and Spokoiny, V. Random gradient-free minimization of convex functions. *Foundations of Computational Mathematics*, 17(2):527–566, 2017.

Ouyang, L., Wu, J., Jiang, X., Almeida, D., Wainwright, C., Mishkin, P., Zhang, C., Agarwal, S., Slama, K., Ray, A., et al. Training language models to follow instructions with human feedback. *Advances in neural information processing systems*, 35:27730–27744, 2022.

Papyan, V. Traces of class/cross-class structure pervade deep learning spectra. *Journal of Machine Learning Research*, 21(252):1–64, 2020.

Radford, A., Wu, J., Child, R., Luan, D., Amodei, D., Sutskever, I., et al. Language models are unsupervised multitask learners. *OpenAI blog*, 1(8):9, 2019.

Rajbhandari, S., Rasley, J., Ruwase, O., and He, Y. Zero: Memory optimizations toward training trillion parameter models. In *SC20: International Conference for High Performance Computing, Networking, Storage and Analysis*, pp. 1–16. IEEE, 2020.

Rang, M., Bi, Z., Zhou, H., Chen, H., Xiao, A., Guo, T., Han, K., Chen, X., and Wang, Y. Revealing the power of post-training for small language models via knowledge distillation. *arXiv preprint arXiv:2509.26497*, 2025.

Sun, T., Shao, Y., Qian, H., Huang, X., and Qiu, X. Black-box tuning for language-model-as-a-service. In *International Conference on Machine Learning*, pp. 20841–20855. PMLR, 2022.

Vaswani, A., Shazeer, N., Parmar, N., Uszkoreit, J., Jones, L., Gomez, A. N., Kaiser, Ł., and Polosukhin, I. Attention is all you need. *Advances in neural information processing systems*, 30, 2017.

Wang, A., Singh, A., Michael, J., Hill, F., Levy, O., and Bowman, S. Glue: A multi-task benchmark and analysis platform for natural language understanding. In *Proceedings of the 2018 EMNLP workshop BlackboxNLP: Analyzing and interpreting neural networks for NLP*, pp. 353–355, 2018.

Wang, A., Pruksachatkun, Y., Nangia, N., Singh, A., Michael, J., Hill, F., Levy, O., and Bowman, S. Super-glue: A stickier benchmark for general-purpose language understanding systems. *Advances in neural information processing systems*, 32, 2019.

Yang, A., Li, A., Yang, B., Zhang, B., Hui, B., Zheng, B., Yu, B., Gao, C., Huang, C., Lv, C., et al. Qwen3 technical report. *arXiv preprint arXiv:2505.09388*, 2025.

Zhang, Y., Li, P., Hong, J., Li, J., Zhang, Y., Zheng, W., Chen, P.-Y., Lee, J. D., Yin, W., Hong, M., et al. Revisiting zeroth-order optimization for memory-efficient llm fine-tuning: A benchmark. In *International Conference on Machine Learning*, pp. 59173–59190. PMLR, 2024.

## Appendix

### A. Proofs

#### A.1. Subspace/Gaussian Smoothing Identities

This section places AGZO and MEZO under one oracle view: each estimator computes (up to  $O(\mu^2)$ ) the gradient of a *smoothed* objective. For AGZO, the smoothing kernel is restricted to a row-subspace; for MEZO it is isotropic.

##### A.1.1. SMOOTHING OPERATORS

Fix a step radius  $\mu > 0$ . For a given layer  $l$ , let  $A_l \in \mathbb{R}^{n_l \times r_l}$  have orthonormal columns ( $A_l^\top A_l = I_{r_l}$ ), and let  $R_l \in \mathbb{R}^{m_l \times r_l}$  have i.i.d.  $\mathcal{N}(0, 1)$  entries. Define the rank- $r_l$  matrix direction  $\Delta_l = R_l A_l^\top$  and the block direction  $\Delta = \{\Delta_l\}_{l=1}^L$ .

**Per-batch and population smoothings.** For a fixed batch  $B$ , define the *subspace smoothing* of  $f(\cdot, B)$ :

$$f_{\mu, A}(W, B) := \mathbb{E}_R[f(W + \mu\Delta, B)], \quad \Delta_l = R_l A_l^\top, \quad R := \{R_l\}_{l=1}^L. \quad (36)$$

Averaging over batches yields the population version

$$F_{\mu, A}(W) := \mathbb{E}_R[F(W + \mu\Delta)] = \mathbb{E}_{B, R}[f(W + \mu\Delta, B)]. \quad (37)$$

For MEZO, let  $U_l \in \mathbb{R}^{m_l \times n_l}$  have i.i.d.  $\mathcal{N}(0, 1)$  entries and set  $\Delta_l = U_l$  (full-dimensional). Define

$$f_{\mu, \text{iso}}(W, B) := \mathbb{E}_U[f(W + \mu\Delta, B)], \quad F_{\mu, \text{iso}}(W) := \mathbb{E}_{B, U}[f(W + \mu\Delta, B)]. \quad (38)$$

##### A.1.2. SUBSPACE-SMOOTHING GRADIENT IDENTITY FOR AGZO

**Lemma A.1** (Gaussian moment identity). *Let  $R \in \mathbb{R}^{m \times r}$  have i.i.d.  $\mathcal{N}(0, 1)$  entries and let  $M \in \mathbb{R}^{m \times r}$  be deterministic. Then*

$$\mathbb{E}[\langle M, R \rangle R] = M, \quad \text{where } \langle M, R \rangle := \text{tr}(M^\top R).$$

Similarly, if  $U \in \mathbb{R}^{m \times n}$  is i.i.d. standard Gaussian and  $G \in \mathbb{R}^{m \times n}$ , then  $\mathbb{E}[\langle G, U \rangle U] = G$ .

*Proof.* We proceed entrywise. For  $a \in \{1, \dots, m\}$  and  $b \in \{1, \dots, r\}$ ,

$$[\mathbb{E}[\langle M, R \rangle R]]_{ab} = \mathbb{E}\left[\left(\sum_{i=1}^m \sum_{j=1}^r M_{ij} R_{ij}\right) R_{ab}\right] = \sum_{i=1}^m \sum_{j=1}^r M_{ij} \mathbb{E}[R_{ij} R_{ab}].$$

Because  $R$  has i.i.d.  $\mathcal{N}(0, 1)$  entries: (i)  $\mathbb{E}[R_{ij}] = 0$  and  $\mathbb{E}[R_{ij}^2] = \text{Var}(R_{ij}) = 1$ ; (ii) if  $(i, j) \neq (a, b)$  then  $R_{ij}$  and  $R_{ab}$  are independent, hence  $\mathbb{E}[R_{ij} R_{ab}] = \mathbb{E}[R_{ij}] \mathbb{E}[R_{ab}] = 0$ . Combining,  $\mathbb{E}[R_{ij} R_{ab}] = 1$  when  $(i, j) = (a, b)$  and 0 otherwise, we have:

$$\mathbb{E}[R_{ij} R_{ab}] = \delta_{ia} \delta_{jb} = \mathbf{1}\{i = a, j = b\}.$$

Using the claim, the double sum collapses to the single surviving term  $M_{ab}$ :

$$[\mathbb{E}[\langle M, R \rangle R]]_{ab} = M_{ab}.$$

Since this holds for every  $(a, b)$ , we have  $\mathbb{E}[\langle M, R \rangle R] = M$ .

The isotropic version is identical: for  $U \in \mathbb{R}^{m \times n}$  i.i.d.  $\mathcal{N}(0, 1)$  and deterministic  $G$ ,

$$[\mathbb{E}[\langle G, U \rangle U]]_{ab} = \sum_{i=1}^m \sum_{j=1}^n G_{ij} \mathbb{E}[U_{ij} U_{ab}] = G_{ab},$$

so  $\mathbb{E}[\langle G, U \rangle U] = G$ .

*Vectorized view.* Let  $z = \text{vec}(R) \sim \mathcal{N}(0, I_{mr})$  and  $x = \text{vec}(M)$ . Then  $\mathbb{E}[(x^\top z)z] = \mathbb{E}[zz^\top]x = I_{mr}x = x$ , which is the same identity reshaped to matrices.  $\square$

**Lemma A.2** (Stein identity for matrix Gaussians). *Let  $R \in \mathbb{R}^{m \times r}$  have i.i.d.  $\mathcal{N}(0, 1)$  entries with joint density  $p(R) = \prod_{a=1}^m \prod_{b=1}^r \phi(R_{ab})$ , where  $\phi(z) = (2\pi)^{-1/2} e^{-z^2/2}$ . Let  $h : \mathbb{R}^{mr} \rightarrow \mathbb{R}$  be  $C^1$  with  $\mathbb{E}|h(R)| < \infty$  and  $\mathbb{E}\|\nabla_R h(R)\|_F < \infty$ . Assume moreover the following sub-Gaussian growth condition:*

(A) *For each coordinate  $(a, b)$ , writing  $U := \{R_{ij} : (i, j) \neq (a, b)\}$  and  $g(z; U) := h(R^{(-ab)}, z)$ , there exist  $\alpha \in (0, \frac{1}{2})$  and a nonnegative random variable  $C(U)$  with  $\mathbb{E}C(U) < \infty$  such that, for all  $z \in \mathbb{R}$ ,*

$$|g(z; U)| + |\partial g(z; U)/\partial z| \leq C(U) e^{\alpha z^2}.$$

Then

$$\mathbb{E}[h(R) R] = \mathbb{E}[\nabla_R h(R)], \quad (39)$$

where the expectation is taken entrywise and  $\nabla_R h$  is the matrix of partial derivatives of  $h$  with respect to the entries of  $R$ .

*Proof.* Fix  $(a, b)$  and let  $Z := R_{ab} \sim \mathcal{N}(0, 1)$ , independent of  $U := \{R_{ij} : (i, j) \neq (a, b)\}$ . Define  $g(z; U) := h(R^{(-ab)}, z)$  with  $R_l^{(-ab)}$  the matrix of fixed other entries, we have  $h(R) = g(Z; U)$ .

Conditioning on  $U$  and using independence of  $Z$  and  $U$ ,

$$\mathbb{E}[h(R) R_{ab}] = \mathbb{E}_U \left[ \mathbb{E}_Z [g(Z; U) Z] \right] = \mathbb{E}_U \left[ \int_{\mathbb{R}} g(z; U) z \phi(z) dz \right].$$

For fixed  $U$  and  $M > 0$ ,

$$\int_{-M}^M g(z; U) z \phi(z) dz = - \int_{-M}^M g(z; U) \phi'(z) dz = -[g(z; U) \phi(z)]_{-M}^M + \int_{-M}^M g'(z; U) \phi(z) dz,$$

since  $\phi'(z) = -z\phi(z)$ . By (A),  $|g(z; U) \phi(z)| \leq C(U) (2\pi)^{-1/2} e^{-(\frac{1}{2}-\alpha)z^2} \rightarrow 0$  as  $|z| \rightarrow \infty$ , so the boundary term vanishes as  $M \rightarrow \infty$ . Dominated convergence (dominated by  $C(U) e^{-(\frac{1}{2}-\alpha)z^2}$ ) yields

$$\int_{\mathbb{R}} g(z; U) z \phi(z) dz = \int_{\mathbb{R}} g'(z; U) \phi(z) dz = \mathbb{E}_Z [g'(Z; U)].$$

By definition of  $g$ ,  $g'(z; U) = \partial h(R)/\partial R_{ab}$  evaluated at the matrix with entry  $(a, b)$  equal to  $z$  and others fixed. Thus

$$\mathbb{E}[h(R) R_{ab}] = \mathbb{E} \left[ \frac{\partial h}{\partial R_{ab}} (R) \right].$$

Stacking over all  $(a, b)$  gives (39).  $\square$

**Theorem A.3** (Restate of Proposition 5.1 and 5.2). *Fix  $W$  and a batch  $B$ . Let  $A_l \in \mathbb{R}^{m_l \times r_l}$  have orthonormal columns, and let  $R_l \in \mathbb{R}^{m_l \times r_l}$  have i.i.d.  $\mathcal{N}(0, 1)$  entries, independently across  $l$ . Define  $\Delta_l := R_l A_l^\top$ ,  $\Delta := \{\Delta_l\}_{l=1}^L$ ,*

$$f_{\mu, A}(W, B) := \mathbb{E}_R f(W + \mu \Delta, B), \quad \phi(W, \Delta; B) := \frac{f(W + \mu \Delta, B) - f(W, B)}{\mu}.$$

Assume  $L$ -smoothness of  $f(\cdot, B)$ . Then for each layer  $l$ :

(a)

$$\nabla_{W_l} f_{\mu, A}(W, B) A_l A_l^\top = \frac{1}{\mu} \mathbb{E}_R [f(W + \mu \Delta, B) R_l A_l^\top]. \quad (40)$$

(b) Using  $\mathbb{E}_R = 0$ ,

$$\nabla_{W_l} f_{\mu, A}(W, B) A_l A_l^\top = \mathbb{E}_R[\phi(W, \Delta; B, B) R_l A_l^\top]. \quad (41)$$

(c) There exist absolute constants  $c_l < \infty$  (depending only on Gaussian moments and layer shapes) such that

$$\left\| \nabla_{W_l} f_{\mu, A}(W, B) A_l A_l^\top - (\nabla_{W_l} f(W, B)) A_l A_l^\top \right\|_F \leq c_l L \mu, \quad (42)$$

Averaging over  $B$  gives the population versions with  $f \rightarrow F$  on both sides.

*Proof.* (a) Let  $h(R) := f(W + \mu\Delta, B)$  with  $\Delta_l = R_l A_l^\top$ . Varying  $R_l$  only, the differential is

$$dh = \langle \nabla_{W_l} f(W + \mu\Delta, B), \mu dR_l A_l^\top \rangle = \mu \langle \nabla_{W_l} f(W + \mu\Delta, B) A_l, dR_l \rangle,$$

hence

$$\nabla_{R_l} h(R) = \mu \nabla_{W_l} f(W + \mu\Delta, B) A_l.$$

By Lemma A.2,

$$\mathbb{E}_{R_l}[h(R) R_l] = \mathbb{E}_{R_l}[\nabla_{R_l} h(R)] = \mu \mathbb{E}_{R_l}[\nabla_{W_l} f(W + \mu\Delta, B) A_l].$$

Right-multiplying by  $A_l^\top$  and dividing by  $\mu$ ,

$$\mathbb{E}_R[\nabla_{W_l} f(W + \mu\Delta, B) A_l A_l^\top] = \frac{1}{\mu} \mathbb{E}_R[f(W + \mu\Delta, B) R_l A_l^\top].$$

By (36), we have:

$$\nabla_{W_l} f_{\mu, A}(W, B) = \mathbb{E}_R[\nabla_{W_l} f(W + \mu\Delta, B)].$$

Hence,

$$\nabla_{W_l} f_{\mu, A}(W, B) A_l A_l^\top = \frac{1}{\mu} \mathbb{E}_R[f(W + \mu\Delta, B) R_l A_l^\top].$$

which is exactly (40).

(b) By  $\mathbb{E}_R = 0$ ,

$$\frac{1}{\mu} \mathbb{E}_R[f(W + \mu\Delta, B) R_l A_l^\top] = \mathbb{E}_R\left[\frac{f(W + \mu\Delta, B) - f(W, B)}{\mu} R_l A_l^\top\right],$$

which yields (41).

(c) By the  $L$ -smooth descent lemma, for  $h = \pm\mu\Delta$ ,

$$f(W+h, B) = f(W, B) + \langle \nabla f(W, B), h \rangle + R_h, \quad |R_h| \leq \frac{L}{2} \|h\|_F^2.$$

Hence

$$\phi(W, \Delta; B, B) = \langle \nabla f(W, B), \Delta \rangle + r_\mu, \quad |r_\mu| \leq \frac{L}{2} \mu \|\Delta\|_F^2.$$

Plugging into (41),

$$\nabla_{W_l} f_{\mu, A}(W, B) A_l A_l^\top = \underbrace{\mathbb{E}_R[\langle \nabla f(W, B), \Delta \rangle R_l A_l^\top]}_{(*)} + \mathbb{E}_R[r_\mu R_l A_l^\top].$$

Evaluate (\*). Decompose layerwise:

$$\langle \nabla f(W, B), \Delta \rangle = \sum_{i=1}^L \langle \nabla_{W_i} f(W, B), R_i A_i^\top \rangle = \sum_{i=1}^L \langle \nabla_{W_i} f(W, B) A_i, R_i \rangle.$$

Therefore

$$(*) = \sum_{i=1}^L \mathbb{E}_R[\langle \nabla_{W_i} f(W, B) A_i, R_i \rangle R_l] A_l^\top.$$

For  $i \neq l$ , independence and  $\mathbb{E}[R_l] = 0$  give zero. For  $i = l$ , apply Lemma A.1 with  $M = \nabla_{W_l} f(W, B) A_l$  and  $R = R_l$  to obtain  $\mathbb{E}[\langle M, R_l \rangle R_l] = M$ , hence  $(*) = \nabla_{W_l} f(W, B) A_l A_l^\top$ .

Bound the remainder. Using  $\|\mathbb{E}[XY]\|_F \leq \mathbb{E}[\|X\| \|Y\|_F]$  and Gaussian moment finiteness,

$$\left\| \mathbb{E}_R[r_\mu R_l A_l^\top] \right\|_F \leq \frac{L}{2} \mu \mathbb{E}[\|\Delta\|_F^2 \|R_l\|_F] \leq c_L L \mu.$$

for some absolute constants  $c_L$ . This yields (42). Averaging over  $B$  proves the population statements.  $\square$

### A.1.3. ISOTROPIC GAUSSIAN SMOOTHING IDENTITY FOR MEZO

**Theorem A.4.** Fix  $W$  and a batch  $B$ . For each layer  $l$ , let  $U_l \in \mathbb{R}^{m_l \times n_l}$  have i.i.d.  $\mathcal{N}(0, 1)$  entries, independently across  $l$ , and define the full-direction block  $\Delta_l := U_l$  and  $\Delta := \{\Delta_l\}_{l=1}^L$ . Define

$$f_{\mu, \text{iso}}(W, B) := \mathbb{E}_U f(W + \mu\Delta, B), \quad \phi(W, \Delta; B, B) := \frac{f(W + \mu\Delta, B) - f(W, B)}{\mu}.$$

Assume  $L$ -smoothness of  $f(\cdot, B)$ . Then for each layer  $l$ :

(a)

$$\nabla_{W_l} f_{\mu, \text{iso}}(W, B) = \frac{1}{\mu} \mathbb{E}_U [f(W + \mu\Delta, B) U_l]. \quad (43)$$

(b) By  $\mathbb{E}_U = 0$ ,

$$\nabla_{W_l} f_{\mu, \text{iso}}(W, B) = \mathbb{E}_U [\phi(W, \Delta; B, B) U_l]. \quad (44)$$

(c) There exist absolute constants  $c_l < \infty$  (depending only on Gaussian moments and layer shapes) such that

$$\|\nabla_{W_l} f_{\mu, \text{iso}}(W, B) - \nabla_{W_l} f(W, B)\|_F \leq c_L L \mu \quad (45)$$

Averaging over  $B$  yields the population versions with  $f \rightarrow F$  on both sides.

*Proof.* (a) By definition, we have:

$$\nabla_{W_l} f_{\mu, \text{iso}}(W, B) = \mathbb{E}_U [\nabla_{W_l} f(W + \mu\Delta, B)].$$

Let  $h(U) := f(W + \mu\Delta, B)$  with  $\Delta_l = U_l$ . Varying  $U_l$  only,

$$dh = \langle \nabla_{W_l} f(W + \mu\Delta, B), \mu dU_l \rangle = \mu \langle \nabla_{W_l} f(W + \mu\Delta, B), dU_l \rangle,$$

so  $\nabla_{U_l} h(U) = \mu \nabla_{W_l} f(W + \mu\Delta, B)$ .

Applying Lemma A.2 to  $U_l$  gives

$$\mathbb{E}_{U_l} [h(U) U_l] = \mathbb{E}_{U_l} [\nabla_{U_l} h(U)] = \mu \mathbb{E}_{U_l} [\nabla_{W_l} f(W + \mu\Delta, B)].$$

Taking expectation over all blocks  $U$  and dividing by  $\mu$  yields

$$\frac{1}{\mu} \mathbb{E}_U [f(W + \mu\Delta, B) U_l] = \mathbb{E}_U [\nabla_{W_l} f(W + \mu\Delta, B)] = \nabla_{W_l} f_{\mu, \text{iso}}(W, B),$$

which is (43).

(b)  $\mathbb{E}_U = 0$  implies

$$\frac{1}{\mu} \mathbb{E}_U [f(W + \mu\Delta, B) U_l] = \mathbb{E}_U \left[ \frac{f(W + \mu\Delta, B) - f(W, B)}{\mu} U_l \right],$$

giving (44).

(c) By the second-order Taylor bounds, for  $h = \pm\mu\Delta$ ,

$$f(W+h, B) = f(W, B) + \langle \nabla f(W, B), h \rangle + R_h, \quad |R_h| \leq \frac{L}{2} \|h\|_F^2.$$

Hence

$$\phi(W, \Delta; B, B) = \langle \nabla f(W, B), \Delta \rangle + r_\mu, \quad |r_\mu| \leq \frac{L}{2} \mu \|\Delta\|_F^2.$$

Insert into (44):

$$\nabla_{W_l} f_{\mu, \text{iso}}(W, B) = \underbrace{\mathbb{E}_U [\langle \nabla f(W, B), \Delta \rangle U_l]}_{(*)} + \mathbb{E}_U [r_\mu U_l].$$

For  $(*)$ , decompose layerwise:

$$\langle \nabla f(W, B), \Delta \rangle = \sum_{i=1}^L \langle \nabla_{W_i} f(W, B), U_i \rangle.$$

Taking expectation, independence across blocks makes cross-terms vanish; for  $i = l$ , apply Lemma A.1 with  $G = \nabla_{W_l} f(W, B)$  and  $U = U_l$  to get  $\mathbb{E}[\langle G, U_l \rangle U_l] = G$ . Thus  $(*) = \nabla_{W_l} f(W, B)$ . Finally,

$$\|\mathbb{E}_U [r_\mu U_l]\|_F \leq \mathbb{E}|r_\mu| \|U_l\|_F \leq c_l L \mu.$$

by finiteness of Gaussian moments, which proves (45). Averaging over  $B$  gives the population statements.  $\square$

#### A.1.4. CONSEQUENCES AND SPECIALIZATIONS

**AGZO.** Let  $S_l^{(r_l)} = \text{span}(U_l^{(r_l)})$  be the leading activation subspace and suppose  $A_l$  is an orthonormal basis that (approximately) spans  $S_l^{(r_l)}$ . By Lemma A.3,

$$\nabla_{W_l} F_{\mu, A}(W) A_l A_l^\top = (\nabla_{W_l} F(W)) A_l A_l^\top + O(L \mu). \quad (46)$$

In the ideal alignment case  $S_l^{(r_l)} = \text{col}(H_l)$ , using  $\text{row}(\nabla_{W_l} F) \subseteq \text{col}(H_l)$  we have  $\nabla_{W_l} F(W) = \nabla_{W_l} F(W) \Pi_{S_l^{(r_l)}}$ , so the only bias comes from smoothing.

**MEZO.** By Lemma A.4,

$$\nabla_{W_l} F_{\mu, \text{iso}}(W) = \nabla_{W_l} F(W) + O(L \mu) \quad (47)$$

Hence MEZO estimates the full (isotropically smoothed) gradient, and is unbiased for  $\nabla F(W)$  as  $\mu \rightarrow 0$ .

## A.2. Expected Cosine Similarity

### A.2.1. EXPECTED COSINE SIMILARITY FOR AGZO

For simplification, we denote the true gradient as  $G \in \mathbb{R}^{m \times n}$  and the agzo approximated gradient as  $\widehat{G}$ . Let  $A \in \mathbb{R}^{n \times r}$  have orthonormal columns ( $A^\top A = I_r$ ) and let  $R \in \mathbb{R}^{m \times r}$  have i.i.d.  $\mathcal{N}(0, 1)$  entries. In AGZO we perturb with

$$\Delta = RA^\top.$$

We assume the smoothing parameter tends to zero  $\mu \rightarrow 0$ , where the central difference in (16) equals the directional derivative:

$$\phi = \langle G, \Delta \rangle = \langle G, RA^\top \rangle.$$

The estimate is

$$\widehat{G}_0 = \phi RA^\top.$$

We use Frobenius inner product  $\langle X, Y \rangle := \text{tr}(X^\top Y)$  and Frobenius norm  $\|X\|_F := \sqrt{\langle X, X \rangle}$ . Our target is the expectation (over  $R$  only)

$$\mathbb{E}_R [\cos(\widehat{G}_0, G)], \quad \cos(X, G) := \frac{\langle X, G \rangle}{\|X\|_F \|G\|_F}.$$

**Theorem A.5** (Copy of Theorem 5.4). *Let  $G \in \mathbb{R}^{m \times n}$  be fixed and  $A \in \mathbb{R}^{n \times r}$  have orthonormal columns. Let  $\hat{G}_0^{\text{AGZO}}$  be the noiseless AGZO estimator constructed from  $\Delta = RA^\top$  with  $R \sim \mathcal{N}(0, I_{m \times r})$ . Then*

$$\mathbb{E}_R [\cos(\hat{G}_0^{\text{AGZO}}, G)] = \beta_{mr} \frac{\|GA\|_F}{\|G\|_F}, \quad (48)$$

where

$$\beta_D := \mathbb{E}[|U_1|], \quad U = (U_1, \dots, U_D) \sim \text{Unif}(\mathbb{S}^{D-1}), \quad (49)$$

depends only on the product dimension  $mr$ . Equivalently,

$$\beta_D = \frac{\Gamma(\frac{D}{2})}{\sqrt{\pi} \Gamma(\frac{D+1}{2})}, \quad (50)$$

and  $\beta_D$  decays on the order of  $1/\sqrt{D}$  as  $D$  increases.

*Proof.* **Step 1 (numerator).** Using  $\langle X, Y \rangle = \text{tr}(X^\top Y)$  and cyclicity of trace,

$$\langle \hat{G}_0, G \rangle = \text{tr}((\phi RA^\top)^\top G) = \phi \text{tr}(AR^\top G) = \phi \text{tr}(R^\top GA) = \phi \langle R, GA \rangle.$$

By definition of  $\phi$ ,

$$\phi = \langle G, RA^\top \rangle = \text{tr}(G^\top RA^\top) = \text{tr}(A^\top G^\top R) = \langle R, GA \rangle.$$

Hence

$$\langle \hat{G}_0, G \rangle = \langle R, GA \rangle^2.$$

**Step 2 (denominator).** We have  $\|\hat{G}_0\|_F = |\phi| \|RA^\top\|_F$ . Since  $A^\top A = I_r$ ,

$$\|RA^\top\|_F^2 = \text{tr}((RA^\top)^\top (RA^\top)) = \text{tr}(AR^\top RA^\top) = \text{tr}(R^\top RA^\top A) = \text{tr}(R^\top R) = \|R\|_F^2.$$

Therefore  $\|RA^\top\|_F = \|R\|_F$  and

$$\|\hat{G}_0\|_F = |\phi| \|R\|_F = |\langle R, GA \rangle| \|R\|_F.$$

**Step 3 (cosine for a fixed  $R$ ).** Combining the two steps,

$$\cos(\hat{G}_0, G) = \frac{\langle \hat{G}_0, G \rangle}{\|\hat{G}_0\|_F \|G\|_F} = \frac{\langle R, GA \rangle^2}{|\langle R, GA \rangle| \|R\|_F \|G\|_F} = \frac{|\langle R, GA \rangle|}{\|R\|_F \|G\|_F}.$$

**Step 4 (vectorization and rotational reduction).** Let  $r := \text{vec}(R) \in \mathbb{R}^d$  with  $d = mr$  and note  $r \sim \mathcal{N}(0, I_d)$ ; also set  $k := \text{vec}(GA)$ , so  $\langle R, GA \rangle = r^\top k$  and  $\|R\|_F = \|r\|_2$ . Thus

$$\cos(\hat{G}_0, G) = \frac{|r^\top k|}{\|r\|_2 \|G\|_F} = \frac{\|k\|_2}{\|G\|_F} \cdot \frac{|r^\top k|}{\|r\|_2}, \quad \hat{k} := \frac{k}{\|k\|_2}.$$

By rotational invariance of  $r \sim \mathcal{N}(0, I_d)$ , the distribution of  $\frac{r}{\|r\|_2}$  is uniform on the unit sphere  $\mathbb{S}^{d-1}$ . Hence

$$\mathbb{E}_R \left[ \frac{|r^\top \hat{k}|}{\|r\|_2} \right] = \mathbb{E}[|U_1|] =: \beta_{mr},$$

where  $U = (U_1, \dots, U_{mr})$  is uniform on  $\mathbb{S}^{mr-1}$ . Therefore

$$\mathbb{E}_R [\cos(\hat{G}_0, G)] = \frac{\|k\|_2}{\|G\|_F} \beta_{mr} = \beta_{mr} \frac{\|GA\|_F}{\|G\|_F}.$$

**Step 5 (closed form for  $\beta_{mr}$ ).** The marginal density of  $U_1$  is

$$f_{mr}(t) = c_{mr} (1 - t^2)^{\frac{mr-3}{2}}, \quad t \in [-1, 1], \quad c_{mr} = \frac{\Gamma(\frac{mr}{2})}{\sqrt{\pi} \Gamma(\frac{mr-1}{2})}.$$

Then

$$\beta_{mr} = \mathbb{E}|U_1| = 2 \int_0^1 t f_{mr}(t) dt = 2c_{mr} \int_0^1 t (1-t^2)^{\frac{mr-3}{2}} dt.$$

With the substitution  $u = t^2$  (so  $du = 2t dt$ ), we get

$$\beta_{mr} = c_{mr} \int_0^1 (1-u)^{\frac{mr-3}{2}} du = c_{mr} \cdot \frac{2}{mr-1} = \frac{\Gamma(\frac{mr}{2})}{\sqrt{\pi} \Gamma(\frac{mr+1}{2})}.$$

□

*Remark A.6* (Equivalent projector form). Since  $A^\top A = I_r$ ,

$$\|GA\|_F^2 = \text{tr}(A^\top G^\top GA) = \text{tr}(G^\top G A A^\top) = \|G A A^\top\|_F^2.$$

Thus the main factor can also be written as  $\|G A A^\top\|_F / \|G\|_F$ , i.e. the fraction of gradient energy captured by the  $r$ -dimensional subspace spanned by the columns of  $A$ .

**Lemma A.7** (Copy of lemma 5.6). *For every integer  $D \geq 2$ , the sequence  $\{\beta_D\}$  is strictly decreasing in  $D$  and satisfies*

$$\sqrt{\frac{2}{\pi D}} \leq \beta_D \leq \sqrt{\frac{2}{\pi(D-1)}}. \quad (51)$$

In particular,  $\beta_{mr} \approx c/\sqrt{mr}$  and  $\beta_{mn} \approx c/\sqrt{mn}$  for a constant  $c \approx \sqrt{2/\pi}$ , so working in a much smaller subspace (with  $r \ll n$ ) already improves the expected cosine similarity by a factor around  $\sqrt{n/r}$ .

*Proof.* By Gautschi's inequality with  $s = \frac{1}{2}$  applied at  $u - \frac{1}{2}$  (so  $u > \frac{1}{2}$ ):

$$\sqrt{u - \frac{1}{2}} < \frac{\Gamma(u + \frac{1}{2})}{\Gamma(u)}.$$

Wendel's inequality (1948) states that for  $u > 0$  and  $s \in (0, 1)$ ,

$$\frac{\Gamma(u+s)}{u^s \Gamma(x)} \leq 1.$$

Set  $s = \frac{1}{2}$  and multiply by  $u^{1/2}$ :

$$\frac{\Gamma(u + \frac{1}{2})}{\Gamma(u)} \leq \sqrt{u} \quad (u > 0).$$

Combining:

$$\sqrt{u - \frac{1}{2}} < \frac{\Gamma(u + \frac{1}{2})}{\Gamma(u)} < \sqrt{u}.$$

Substituting  $u = \frac{D}{2}$  and multiplied by  $\sqrt{\pi}$ , we get:

$$\sqrt{\frac{\pi(D-1)}{2}} < \frac{1}{\beta_D} < \sqrt{\frac{\pi D}{2}}$$

By reversing we complete the proof. □

### A.3. AGZO defeat MEZO in cosine similarity

We compare the noiseless expectations from theorem 5.4 and corollary 5.5:

$$\mathbb{E}_R \left[ \cos(\hat{G}_0^{\text{AGZO}}, G) \right] = \beta_{mr} \frac{\|GP_A\|_F}{\|G\|_F}, \quad \mathbb{E}_R \left[ \cos(\hat{G}_0^{\text{MEZO}}, G) \right] = \beta_{mn},$$

where  $A \in \mathbb{R}^{n \times r}$  is orthonormal (AGZO's subspace),  $P_A = AA^\top$ , and

$$\beta_D = \frac{\Gamma(\frac{D}{2})}{\sqrt{\pi} \Gamma(\frac{D+1}{2})} \quad (D \in \mathbb{N}).$$

Define the *energy-capture factor*

$$\alpha(A; G) := \frac{\|GP_A\|_F}{\|G\|_F} \in [0, 1].$$

Then

$$\mathbb{E}_R \left[ \cos(\hat{G}_0^{\text{AGZO}}, G) \right] > \mathbb{E}_R \left[ \cos(\hat{G}_0^{\text{MEZO}}, G) \right] \iff \alpha(A; G) > \frac{\beta_{mn}}{\beta_{mr}}. \quad (52)$$

The threshold is the *exact* constant

$$\frac{\beta_{mn}}{\beta_{mr}} = \frac{\Gamma(\frac{mn}{2})}{\Gamma(\frac{mr}{2})} \cdot \frac{\Gamma(\frac{mr+1}{2})}{\Gamma(\frac{mn+1}{2})}.$$

By lemma 5.6, we have

$$\frac{\beta_{mn}}{\beta_{mr}} < \frac{\sqrt{\frac{mr}{2}}}{\sqrt{\frac{mn}{2} - \frac{1}{2}}} = \frac{\sqrt{mr}}{\sqrt{mn - 1}}.$$

Hence AGZO beats MEZO if,

$$\alpha(A; G) > \frac{\sqrt{mr}}{\sqrt{mn - 1}}$$

or (by equation (31))

$$\frac{\sum_{i=1}^r B_{ii} \sigma_i^2}{\sum_{i=1}^s B_{ii} \sigma_i^2} > \frac{r}{n - 1/m} \quad (53)$$

We then have the following theorem to see (53) is valid if  $B$  is isotropic.

**Theorem A.8** (Copy of theorem 5.7). *Consider a layer with gradient factorization  $\nabla_{W_\ell} F(W) = Q_\ell H_\ell^\top$  and compact SVD  $H_\ell = U_\ell \Sigma_\ell V_\ell^\top$  of rank  $s_\ell < n_\ell$  with singular values  $\{\sigma_{\ell,i}\}_{i=1}^{s_\ell}$ . Let  $A_\ell = U_\ell^{(r_\ell)}$  be the AGZO subspace and  $B_\ell = V_\ell^\top Q_\ell^\top Q_\ell V_\ell$ . If the average of its first  $r$  diagonal entries is not less than the average of all diagonal entries, i.e.,*

$$\frac{1}{r_\ell} \sum_{i=1}^{r_\ell} B_{\ell,ii} \geq \frac{1}{s_\ell} \sum_{i=1}^{s_\ell} B_{\ell,ii}, \quad (54)$$

and that  $H_\ell$  is low-rank, i.e.,  $s_\ell < n_\ell$ . Then

$$\frac{\sum_{i=1}^{r_\ell} B_{\ell,ii} \sigma_{\ell,i}^2}{\sum_{i=1}^{s_\ell} B_{\ell,ii} \sigma_{\ell,i}^2} > \frac{r_\ell}{s_\ell} \geq \frac{r_\ell}{n_\ell - 1/m_\ell}, \quad (55)$$

and hence, in the noiseless single-query setting,

$$\mathbb{E}_R \left[ \cos(\hat{G}_0^{\text{AGZO}}, G_\ell) \right] > \mathbb{E}_R \left[ \cos(\hat{G}_0^{\text{MEZO}}, G_\ell) \right]. \quad (56)$$

Moreover, when the singular values  $\{\sigma_{\ell,i}\}$  are more heterogeneous (so that the leading directions carry more weighted energy), the gap in expected cosine similarity becomes larger.

*Proof.* Here we omit the subscript  $\ell$  for simplicity. Define

$$D := \frac{1}{r} \sum_{i=1}^r B_{ii} \sigma_i^2 - \frac{1}{s} \sum_{i=1}^s B_{ii} \sigma_i^2 = \frac{s-r}{rs} \sum_{i=1}^r B_{ii} \sigma_i^2 - \frac{1}{s} \sum_{i=r+1}^s B_{ii} \sigma_i^2.$$

Since  $\sigma_1 > \dots > \sigma_s \geq 0$ , we have for  $i \leq r$  that  $\sigma_i^2 \geq \sigma_r^2$ , and for  $r < i \leq s$  that  $\sigma_i^2 \leq \sigma_{r+1}^2$ . Hence

$$D \geq \frac{s-r}{rs} \sigma_r^2 \sum_{i=1}^r B_{ii} - \frac{1}{s} \sigma_{r+1}^2 \sum_{i=r+1}^s B_{ii}.$$

Add and subtract  $\frac{s-r}{rs} \sigma_{r+1}^2 \sum_{i=1}^r B_{ii}$  to obtain

$$D \geq \frac{1}{rs} \left( s \sum_{i=1}^r B_{ii} - r \sum_{i=1}^s B_{ii} \right) \sigma_{r+1}^2 + \frac{s-r}{rs} (\sigma_r^2 - \sigma_{r+1}^2) \sum_{i=1}^r B_{ii}.$$

By the assumption,

$$s \sum_{i=1}^r B_{ii} - r \sum_{i=1}^s B_{ii} = rs \left( \frac{1}{r} \sum_{i=1}^r B_{ii} - \frac{1}{s} \sum_{i=1}^s B_{ii} \right) \geq 0.$$

Moreover,  $\sigma_r^2 - \sigma_{r+1}^2 > 0$  and  $B_{ii} \geq 0$ . Therefore both terms on the right-hand side are nonnegative, which yields  $D \geq 0$ , or equivalently,

$$\frac{\sum_{i=1}^r B_{ii} \sigma_i^2}{\sum_{i=1}^s B_{ii} \sigma_i^2} > \frac{r}{s} \geq \frac{r}{n-1/m}.$$

The second inequality is due to the fact that  $s < n$  and both  $s, n \in \mathbb{N}^+$ . Combining with equation (53) and (52), we can conclude that AGZO generally can get gradient estimation have larger cosine similarity with the true gradient than MEZO.  $\square$

## B. Detail of Pangu Model Experiments

This section presents our additional experimental results of PANGU-1B model on Ascend NPU.

**Model.** To evaluate the generality of our approach across different model architectures, we further conduct experiments on the openPangu family of models. The openPangu series has demonstrated strong performance on a wide range of general language understanding and sophisticated reasoning tasks (Rang et al., 2025; Chen et al., 2025a). In particular, we select OPENPANGU-EMBEDDED-1B<sup>1</sup>, a model specifically designed for efficient inference on edge devices (we use the GPU variant in our experiments<sup>2</sup>).

**Evaluation Setup.** Under the same experimental setup as described in the main pages, we conduct evaluations on OPENPANGU-EMBEDDED-1B using SuperGLUE (Wang et al., 2019) and additional datasets, with identical baseline comparisons. All training experiments are conducted on a server running Ubuntu 22.04, equipped with 96GB RAM and two NVIDIA RTX 3090 GPUs. For inference evaluation, in addition to the GPU platform described above, we also perform evaluations on a high-memory NPU server configured with 1.5 TB of RAM and  $8 \times 64$  GB 910B2 NPUs running EulerOS 2.0.

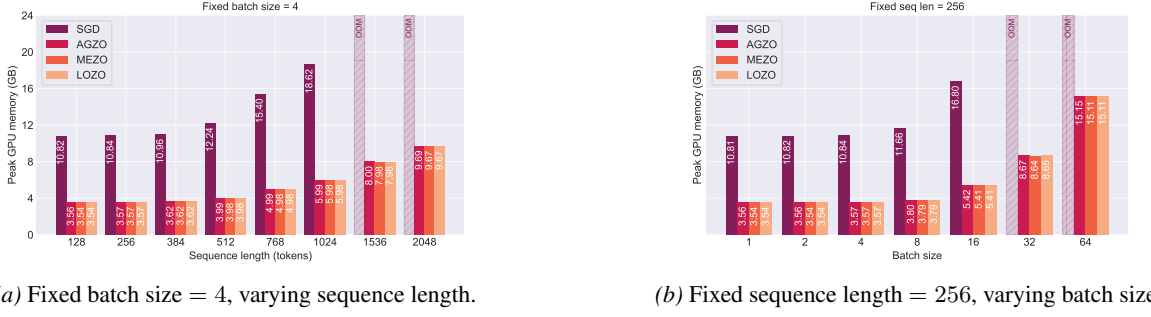
**Training Details.** Regarding numerical precision, unlike the main experiments where the Qwen models are loaded in FP32 precision, we load the openPangu models using BF16 precision. Since FP32 has 16 more mantissa bits than BF16, zeroth-order optimization requires a perturbation magnitude that is 2–3 orders of magnitude larger when using BF16 compared to FP32. Accordingly, for the openPangu models, we set the zeroth-order perturbation parameter to  $ZO\_EPS = 1 \times 10^{-4}$ . We adopt the same experimental configurations, i.e., training, preprocessing, evaluation, and hyperparameter tuning setup as described in Section 6.

### B.1. End-to-end cross-platform fine-tuning performance

We evaluate the cross-platform inference performance, i.e., evaluating the performance on NPU with GPU-trained models. Table 3 presents the performance of AGZO and various baselines on OPENPANGU-EMBEDDED-1B across on NPU. Across

<sup>1</sup><https://huggingface.co/FreedomIntelligence/openPangu-Embedded-1B>

<sup>2</sup><https://modelscope.cn/models/wangrongsheng/openPangu-Embedded-1B-model-GPU>



(a) Fixed batch size = 4, varying sequence length.

(b) Fixed sequence length = 256, varying batch size.

Figure 4. Peak GPU memory usage when fine-tuning Pangu-1B on DROP.

both GPU and NPU, AGZO consistently achieves the best results among zeroth-order methods and non-training baselines on most downstream tasks. On the NPU, AGZO attains an average score of 0.709, outperforming other ZO baselines on tasks such as SST2, COPA, BoolQ, RTE, and WiC. The slightly lower performance on the NPU compared to the GPU may be attributed to subtle differences in numerical precision, memory layout, or low-level kernel implementations, which can affect the propagation of small perturbations used in zeroth-order optimization.

Table 3. Experiments on Pangu-1B(NPU). The best results are shown in bold except for FO.

Task	FO	AGZO	MEZO	LOZO	Zero	ICL
SST2	0.821	0.765	<b>0.766</b>	0.718	0.571	0.710
COPA	0.800	<b>0.770</b>	0.740	0.720	0.760	0.740
CB	0.696	0.696	<b>0.732</b>	0.643	0.482	0.446
BoolQ	0.752	<b>0.728</b>	0.697	0.694	0.696	0.731
RTE	0.780	<b>0.729</b>	<b>0.729</b>	0.682	0.578	0.682
WiC	0.657	<b>0.567</b>	0.552	0.542	0.469	0.495
Avg.	0.738	<b>0.709</b>	0.703	0.667	0.593	0.636

## B.2. Peak GPU memory footprint

We empirically validate our memory efficiency analysis by measuring the peak GPU memory footprint of fine-tuning PANGU-1B on the DROP task. The comparative results are presented in Figure 4. In Figure 4a, we fix the batch size at 4 and scale the sequence length. While the First-Order (FO) baseline (SGD) encounters Out-Of-Memory (OOM) errors at a sequence length of 1,536, AGZO maintains a strictly linear scaling, consuming only 9.69 GB even at a length of 2,048.

Moreover, in the second setting with a fixed sequence length of 256 (Figure 4b), SGD triggers OOM at a batch size of 32, whereas AGZO remains operative up to a batch size of 64 ( $\approx 15.15$  GB).

The experimental results demonstrate that the memory trajectory of AGZO aligns almost perfectly with other forward-only zero-order baselines (i.e., MEZO and LOZO). This evidence substantiates that the additional computation required for our activation-guided subspace construction introduces negligible memory overhead, preserving the inherent memory advantages of ZO optimization.